J. Fluid Mech. (1974), *vol.* 65, *part* 1, *pp.* 153–175
Printed in Great Britain

Mixing layers for highly underexpanded supersonic jets in hypersonic streams

By JAMES P. MORAN

Aerodyne Research, Inc., Burlington, Massachusetts 01803

(Received 30 November 1973 and in revised form 6 February 1974)

The mixing layer bounding the exhaust plume associated with hypersonic high-altitude rockets is analysed as a laminar binary mixture of perfect gases with Lewis and Prandtl numbers of unity. A far-field approximation to the undisturbed jet core and a Newtonian pressure balance between the jet and ambient gases are used to construct the mixing-layer location. Longitudinal pressure variations are neglected and resultant errors are evaluated. Boundary conditions at the edge of the mixing layer are evaluated by streamline tracing to shock entry points. The sensitivity of properties in the mixing layer to variations in the plume angle of attack, engine nozzle efficiency and engine thrust are examined, and an approximate density and thrust scaling of mixing-layer overall properties is developed.

1. Introduction

An important contribution to the radiation signature of booster rockets at high altitudes comes from the mixing layer at the exhaust-plume boundary between the stream and jet gases. Analysis of the radiation in terms of dominant thermal and chemical processes must be based on a reasonably accurate fluid-mechanical description of the gas flow field in the mixing layer. If the mixing layer is thin compared with the plume scale, major simplifications apply to its flow description at high altitudes, because the vehicle flight Mach number is large (> 5) and the flow at the rocket nozzle exit is highly underexpanded. Hypersonic vehicle flight implies that the stream temperature $\bar{T}_\infty$ and, hence, the stream Mach number $\bar{M}_\infty$ have only a weak influence on plume structure in relatively blunt portions of the plume. Highly underexpanded nozzle flow implies that a major portion of the plume is relatively blunt, and also that undisturbed jet flow at large distances from the nozzle provides a complete description of jet-gas influence on plume structure.

Several approximate models have been proposed for the distant undisturbed jet flow of ideal gases from nozzles with uniform exit conditions. Distant flow-field properties are described entirely by the local density and nozzle conditions, since the local speed has very nearly its maximum value $\bar{q}_m$. The distant jet density is modelled by an $\bar{r}^{-2}$ decrease with distance and a functional vibration with the polar angle θ from the nozzle axis. These models are governed by two parameters evaluated from mass conservation and either momentum conservation or the exit Prandtl–Meyer function. Ashkenas & Sherman (1966) modelled the experimental

data of Hartmann & Lazarus (1941) and the method of characteristics (MOC) solution of Owen & Thornhill (1948) using a variation in density with the polar angle θ as $\cos^2\theta$. Their two-parameter model applies in the limit of sonic nozzle-exit conditions. Mirels & Mullen (1962) considered a jet density variation near the limit $M_e \to \infty$ of infinite nozzle-exit Mach number. Their analysis, by application of the hypersonic equivalence of Hayes (1947), is based on an approximate extension of the description by Sedov (1959) of self-similar expansions of cylindrical gas clouds into a vacuum. For the cases considered, their results are in agreement to within 10% with MOC calculations. For intermediate values of M_e, Alden, Habert & Hill (1963), Albini (1965) and Hubbard (1966) have modelled the distant density angular variation as $[\cos(\pi\theta/2\theta_m)]^{1/(\gamma_j-1)}$, where γ_j is the jet specific-heat ratio and θ_m is the exit maximum turning angle. Boynton (1967) and Thomson (1965) showed that this function squared provided a better fit to the θ dependence of the density, by comparison with several numerical computations. Hill & Draper (1966) obtained good agreement with the numerical solutions of Thomson (1965), Altshuler, Moe & Molund (1958) and Sibulkin & Gallaher (1963) for a wide variety of nozzle conditions, using the model

$$\bar{\rho}/\bar{\rho}_{\mathbb{Q}} = \exp(-\Lambda^2\beta^2), \tag{1.1}$$

where $\bar{\rho}_{\mathbb{Q}}$ is the density at $\theta = 0$ and $\beta = 1-\cos\theta$.

Conservation of mass and momentum provides the relations

$$\left.\begin{aligned} \Lambda^{-1} &= \pi^{\frac{1}{2}}(1 - C_F/C_{FM}) \\ \text{and} \qquad \bar{\rho}_{\mathbb{Q}}/\bar{\rho}_c &= 4B(\bar{r}^*/\bar{r})^2, \end{aligned}\right\} \tag{1.2}$$

where
$$C_F = \bar{T}/(\bar{p}_c\pi\bar{r}^{*2}), \quad C_{FM} = \bar{M}\bar{q}_m/(\bar{p}_c\pi\bar{r}^{*2}),$$
$$B = [2/(\gamma_j+1)]^{1/(\gamma_j-1)}[\Lambda/(16\pi)^{\frac{1}{2}}][(\gamma_j-1)/(\gamma_j+1)]^{\frac{1}{2}},$$

$\bar{p}_c$ is the chamber density, $\bar{r}^*$ the throat radius, $\bar{T}$ the engine vacuum thrust, $\bar{p}_c$ the chamber pressure and $\bar{M}$ the nozzle mass flow rate.

Boynton (1968) has compared the numerical solutions for undisturbed jet expansions from nozzles with and without wall boundary layers. These show that, even for the largest booster engines, the nozzle boundary layer has an important effect on distant jet flow at large angles ($\sim 90°$) to the nozzle axis. Boynton observed that the density variation with θ is approximately exponential in the region of significant boundary-layer influence, and on this basis Simons (1972) applied an approximate correction to inviscid flow.

Radiation observations of high-altitude rocket plumes, reported by Rosenberg *et al.* (1961), prompted the analyses of Thomson & Harshbarger (1961), and later Hill & Habert (1963) and Alden & Habert (1964), which showed a dominant high-altitude plume scale $\bar{L}$, equal to the square root of the engine vacuum thrust divided by the stream dynamic pressure. Moran (1967) showed by dimensional arguments that, for fixed nozzle geometry and stream and jet specific-heat ratios γ_∞ and γ_j, the high-altitude, inviscid plume geometry scales with $\bar{L}$. Hill & Habert developed axial transverse scaling of plume geometry, based on the blast-wave theory of Sedov (1959) and Taylor (1950), as

$$x = \bar{x}/\bar{L}, \quad y = \bar{y}/\bar{L}(\bar{D}/\bar{T})^{\frac{1}{4}}, \tag{1.3}$$

where $\bar{L} = (\bar{T}/\bar{Q}_\infty)^{\frac{1}{2}}$, $\bar{Q}_\infty = \frac{1}{2}\bar{\rho}_\infty\bar{q}_\infty^2$, $\bar{\rho}_\infty$ is the stream density, $\bar{q}_\infty$ is the vehicle

speed and $\bar{D}$ is the plume pressure drag. This scaling was used in developing the so-called universal plume model of Jarvinen & Hill (1970), empirically based as well on numerical solutions and flight observations. By a simple but approximate momentum balance, the plume drag was related to engine conditions by Hill & Habert (1963) by

$$\bar{D}/\bar{T} = C_{FM}/C_F - 1. \tag{1.4}$$

Thus all engine and flight characteristics are contained only in the dimensionless plume co-ordinates of (1.3). Blast-wave theory may strictly be applied to jet external flow only when outer shock and contact-surface inclinations to the free stream are small and shock normal Mach numbers are large, conditions not applying to high-altitude plumes; consequently, the validity of the $\bar{D}/\bar{T}$ scaling in (1.3) is in doubt. Draper & Moran (1973*a*) have shown that this scaling fails when $\bar{D}/\bar{T}$ is very small. However, this quarter-power dependence of $\bar{D}/\bar{T}$ suggests a rather weak influence of nozzle conditions (other than thrust) on inviscid plume geometry, and the Jarvinen–Hill model has broad utility in describing both scaled simulations and actual high-altitude plumes (see Draper & Moran 1973*a*, *b*; Jarvinen & Dyner 1969).

Large stream Mach numbers and large plume dimensions suggest the calculation of high-altitude plume contact-surface locations on the basis of a pressure balance by the use of the Newtonian approximation for both internal and external flows. Using the undisturbed jet flow model of Alden *et al.* (1963), this was first done by Alden & Habert (1964), who approximately accounted for centrifugal pressure relief across both inner and outer shock layers by assuming a homogeneous layer between shocks. Albini (1965) modified this analysis by allowing separate homogeneous inner and outer shock layers. Hubbard (1966) further improved the model by allowing laminar shock layers with the speed assumed constant along post-shock streamlines. Using his model for undisturbed jet flow, Boynton (1967) applied Hubbard's method, with centrifugal pressure relief neglected in the outer shock layer. Hayes & Probstein (1959) and Chernyi (1961) reported the observations that Newtonian flow theory provided a better comparison with measured surface pressures on convex surfaces (contact surfaces) when outer shock-layer pressure relief was neglected. Draper & Moran (1973*b*) followed Hubbard's method of contact-surface development, but used the Hill–Draper (1966) model for undisturbed jet flow; this construction is used in the present mixing-layer analysis. A comparison is shown in figure 1 of contact-surface locations from the Jarvinen–Hill (1970) model, from Hubbard's method constructed using the undisturbed jet models of Boynton (1967) and Hill & Draper (1966), and from the multi-tube numerical solution reported by Boynton. All these methods are in reasonable agreement except in the blunt nose region, where the Jarvinen–Hill form is significantly different from the others. It is noted that, if the others were to account for nozzle boundary-layer effects, they would be in closer agreement with the semi-empirical model of Jarvinen & Hill.

With the assumption of thin shock layers, implied by the Newtonian flow construction of the inviscid contact surface, it is consistent to formulate the viscous mixing-layer flow under the assumption of a thin boundary layer. Considerable attention must be given to mixing-layer boundary conditions for a high-altitude

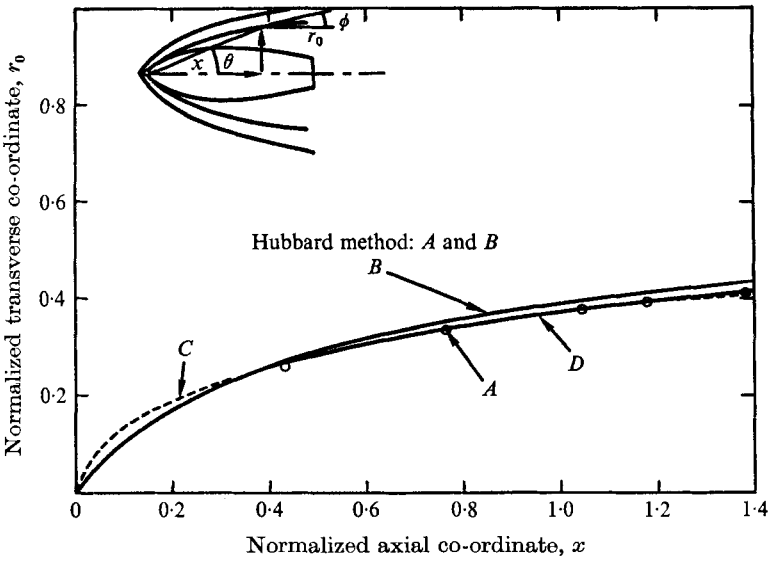

FIGURE 1. Comparison of inviscid contact-surface models (A, B and C) with a numerical solution (D). (See Boynton (1967) for A and D, equation (2.3) for B, and Jarvinen & Hill (1970) for C.) $\gamma_j = 1{\cdot}22$, $\gamma_\infty = 1{\cdot}4$, $M_e = M_\infty = 4{\cdot}0$, $\alpha = 0$.

plume, since the layer thickness may not be small compared with the shock-layer thickness. The formulation of boundary-layer equations in self-similar form for a binary mixture of non-reacting perfect gases is well established (Dorrance 1962). The same formulation applies to thin mixing layers, although the boundary conditions and the limitations imposed by self-similarity are different (Greenberg 1966).

Greenberg argued that, with longitudinal pressure gradients, self-similar mixing-layer solutions exist only when both gases have the same specific-heat ratio and stagnation pressure. These conditions provide a relationship between the ratio of velocities across the layer and the ratio of stagnation enthalpies across the layer, so that mixing-layer solutions depend only on the pressure gradient and the velocity ratio. Casaccio (1963) obtained self-similar solutions to mixing-layer equations for a reacting gas, in apparent violation of the restrictions discussed by Greenberg. However, the pressure-gradient term of both Greenberg and Casaccio vanishes at both edges of the mixing layer, suggesting that its influence may be small. This very weak pressure-gradient effect is illustrated in Casaccio's solution, and points to the approximate validity of the local self-similarity concept used extensively in boundary-layer analysis (Hayes & Probstein 1959).

Lock (1951) observed that self-similar shear-layer solutions satisfied the three-point boundary conditions under an arbitrary transverse displacement as large as the layer thickness. Ting (1959) showed that the transverse location was determined by applying the transverse momentum equation of the lowest order containing shear-layer influence on the external flow. Greenberg's stagnation-region solutions show that the dividing stream surface is displaced from the inviscid

contact surface by a fraction of the mixing-layer thickness. Consequently, in the present work these surfaces are assumed to coincide. The transverse momentum equation, however, is retained in the present plume mixing-layer study, because the pressure varies strongly across the inner shock layer.

Concurrent with the plume analyses reviewed above was the development of detailed finite-difference treatments of some or all of the flow regions associated with high-altitude plumes. The present state of these efforts is described by the recent work of Boynton (1971) and Wilson (1973), who have carried out axisymmetric viscous flow computations, and of Rudman (1973), who has carried out three-dimensional inviscid flow computations. The neglect of cross-flow, implicit in the present analysis of the inviscid inner shock layer in the plane of symmetry for plumes at an angle of attack, is supported by Rudman's results.

In the present work an analytically and computationally tractable treatment of plume mixing layers and shock layers is developed. Local shock-layer properties are used as the boundary conditions for the edge of a mixing layer to allow the proper description of the mixing layer, even when it occupies a substantial fraction of the region between the inner and outer plume shocks. Neglect of the longitudinal pressure gradient is shown to be consistent with the flow features peculiar to high-altitude plumes. This important simplification relaxes the restrictions on self-similarity discussed by Greenberg, and allows Crocco integral solutions to simplified forms of the energy and species equations. This treatment yields very simple forms for important mixing-layer and shock-layer properties.

2. Inviscid contact surface

This plume mixing-layer analysis applies for axisymmetric flow, and in the plane of symmetry when the thrust axis is at an angle of attack α relative to flight direction. With the sign convention of figure 2, the undisturbed jet flow is modelled by (1.1) and (1.2) in the plane of symmetry if θ is replaced by $\theta+\alpha$. The contact surface is constructed by equating the pressures and flow directions of the jet and stream gases, and approximating the pressure on both sides by Newtonian theory. In the outer flow, centrifugal pressure relief across the shock layer is neglected, and the Newtonian pressure is modified to equal the stagnation-point value predicted by the constant-density solution of Li & Geiger (1957),

$$\bar{p}_{cs} = \bar{Q}_\infty[(\gamma_\infty+3)(\gamma_\infty+1)^{-1}\sin^2\phi + 2(\gamma_\infty M_\infty^2)^{-1}]. \tag{2.1}$$

In the inner flow, Newtonian theory is applied with inclusion of the Busemann centrifugal pressure correction to yield

$$\bar{p}_{cs} = \bar{\rho}\bar{q}_m^2\sin^2(\theta-\phi) - \sin\phi\left(\frac{d\phi}{d\bar{r}_0}\right)\int_0^{\bar{r}_0}\tilde{\bar{\rho}}\tilde{\bar{q}}_m^2\frac{\tilde{\bar{r}}\sin\tilde{\theta}}{\bar{r}\sin\theta}\frac{\sin^2(\tilde{\theta}-\tilde{\phi})}{2\sin\tilde{\phi}}d\tilde{\bar{r}}_0, \tag{2.2}$$

where a tilde indicates an integration variable. Equations (2.1), (2.2) and (1.2) provide an ordinary differential equation describing the contact-surface location,

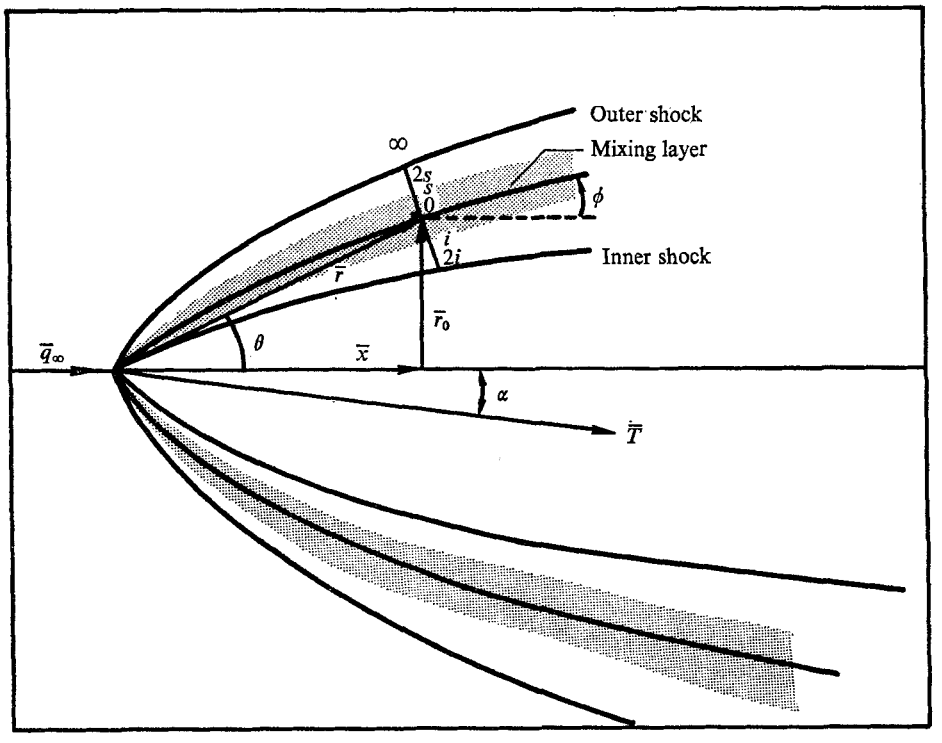

FIGURE 2. Plume geometry in the plane of symmetry.

which may be reduced, using isentropic nozzle-flow relations and the hypersonic scale $\bar{L}$, to

$$R_c = \frac{rLI}{\sin\theta}\left[r^2\left(\frac{1}{2}\frac{\gamma_\infty+3}{\gamma_\infty+1}\sin^2\phi+\frac{1}{\gamma_\infty M_\infty^2}\right)-L\exp\left(-\Lambda^2\beta^2\right)\sin^2(\theta-\phi)\right]^{-1}, \tag{2.3}$$

where unbarred lengths are normalized by $\bar{L}$, $\beta = 1-\cos(\theta+\alpha)$, $\bar{R}_c$ is the local radius of curvature,

$$L = \Lambda[1+\tfrac{1}{2}(\gamma_j-1)M_e^2]^{\frac{1}{2}}[2(\gamma_j-1)\pi^3 M_e^2]^{-\frac{1}{2}}(1+\gamma_j^{-1}M_e^{-2})^{-1}$$

and

$$I = \int_\theta^\pi \exp\left(-\Lambda^2\tilde{\beta}^2\right)\sin\tilde{\theta}\cos(\tilde{\theta}-\tilde{\phi})\,d\tilde{\theta}.$$

The solution to (2.3) is started away from the origin, at a selected small value of $\theta-\phi$. The contact surface is assumed to have slopes at the origin in the plane of symmetry of $\pm\frac{1}{2}\pi\pm\frac{1}{2}\alpha$ on the windward and leeward sides, respectively, for plumes at an angle of attack. Corresponding starting values for r, R_c, θ and ϕ are determined from the geometry and (2.3). Typically, for a starting $\theta-\phi$ of 10^{-3} rad, $r\sim 10^{-6}$ and $R_c\sim 10^{-3}$; consequently, the complex contact-surface geometry predicted by (2.3) closer to the origin is on so small a scale as to be irrelevant for the present study . The contact surface predicted by (2.3) is shown in figure 1 to be in good agreement with the numerical solution reported by Boynton (1967).

3. Mixing-layer equations

With $\bar{s}$ as the distance from the source along the contact surface and $\bar{y}$ as the distance inward normal to the contact surface, the momentum equations along and across the mixing layer take the following forms, after thin-layer simplifications:

$$\bar{\rho}\bar{u}\,\partial\bar{u}/\partial\bar{s} + \bar{\rho}\bar{v}\,\partial\bar{u}/\partial\bar{y} = -\partial\bar{p}/\partial\bar{s} + \partial(\bar{\mu}\,\partial\bar{u}/\partial\bar{y})/\partial\bar{y}, \tag{3.1}$$

$$\partial\bar{p}/\partial\bar{y} = -\bar{\rho}\bar{u}^2/\bar{R}_c, \tag{3.2}$$

where $\bar{u}$ and $\bar{v}$ are $\bar{s}$ and $\bar{y}$ velocity components, respectively, and $\bar{\mu}$ is the viscosity coefficient. Solutions are sought for the stream function given by

$$\partial\bar{\psi}/\partial\bar{y} = \bar{\rho}\bar{u}\bar{r}_0, \quad \partial\bar{\psi}/\partial\bar{s} = -\bar{\rho}\bar{v}\bar{r}_0, \tag{3.3}$$

which identically satisfies the axisymmetric mass-conservation equation. Note that an axisymmetry formulation is valid for plumes at an angle of attack in the plane of symmetry, if one assumes negligible girth-wise spreading of streamlines within the thin shock layers near this plane. Self-similar solutions are sought by separation of the variables in $\bar{\psi}$ as

$$\bar{\psi} = \bar{N}(\bar{s})f(\eta), \quad \bar{u} = \bar{u}_i f'(\eta), \tag{3.4}$$

where the subscript i indicates conditions along the inner edge of the mixing layer. Substitution of (3.4) into (3.1) shows

$$\bar{N}(\bar{s}) = \left(2\int_0^{\bar{s}} \bar{\rho}_s\bar{\mu}_s\bar{u}_i\bar{r}_0^2\,d\bar{s}\right)^{\frac{1}{2}}$$

to be the required form to allow self-similar solutions (Dorrance 1962). With this, and the following choice of normalization,

$$\left.\begin{aligned} \rho = \bar{\rho}/\bar{\rho}_\infty, \quad \mu = \bar{\mu}(M_\infty\bar{\mu}_\infty)^{-1}, \quad p = \bar{p}/\bar{Q}_\infty, \\ \tilde{s} = \int_0^s \rho_s\mu_s u_i r_0^2\,ds, \quad q = \bar{q}/\bar{q}_m, \quad \eta = [Re\,(2M_\infty\tilde{s})^{-1}]^{\frac{1}{2}}\int_0^y \rho\,dy, \end{aligned}\right\} \tag{3.5}$$

where $Re = \bar{\rho}_\infty\bar{q}_m\bar{L}/\bar{\mu}_\infty$ and the subscript s indicates the outer edge of the mixing layer, (3.1) and (3.2) become

$$(Cf'')' + ff'' = (\partial\ln\tilde{s}/\partial s)^{-1}[q_\infty^2(\partial p/\partial s)(\rho u_i^2)^{-1} + 2f'^2\partial\ln u_i/\partial s], \tag{3.6}$$

$$p = p_{cs} - 2q_\infty^{-2}\left(\frac{M_\infty}{Re}\right)^{\frac{1}{2}}\frac{u_i(2\tilde{s})^{\frac{1}{2}}}{r_0R_c}\int_0^\eta f'^2\,d\eta, \tag{3.7}$$

where $C = \rho\mu/\rho_s\mu_s$. Transverse variations in pressure are included in (3.6) and (3.7) because large transverse pressure gradients appear in the inviscid treatment of the thin inner shock layer. Contact-surface and post-inner-shock pressures may differ by almost an order of magnitude. The viscosity in the outer shock layer is assumed to vary linearly with temperature along the edge of the mixing layer and about a reference value of $8{\cdot}5\times10^{-5}$ kg/ms at 3000 °K. This assumption allows a simple evaluation of $\tilde{s}$, since $\rho_s\mu_s$ is proportional to p_{cs}. The free-stream viscosity is not required in the analysis; however, the normalization $\bar{\mu}_\infty M_\infty$ was chosen to identify M_∞ and Re dependencies for scaling. Since $\bar{\mu}$ varies more nearly like

$\bar{T}^{\frac{1}{2}}$, this dependence is assumed for the large temperature variations between the stream and the shock layer, and the above normalization yields a dimensionless viscosity insensitive to flight conditions when M_∞ is large.

Consistent with the assumption of a thin shock layer, the $\bar{s}$ velocity component downstream of the inner shock is approximately $\bar{q}_m \cos(\theta - \phi)$, and does not change greatly along shock-layer streamlines. The contact-surface equation (2.3) and figure 1 show that $\theta - \phi$ is everywhere small. Consequently, u_i is nearly constant throughout the inner shock layer, and the second term on the right-hand side of (3.6) may be neglected. Furthermore, if we view the contact-surface pressure as representative of the mixing layer, $\partial p/\partial s$ is small for θ close to $\frac{1}{2}\pi$, since p has a maximum at $\frac{1}{2}\pi$, and also $\partial p/\partial s$ approaches zero as $\phi \to \theta$. From the Newtonian pressure relation, the pressure gradient $\partial p/\partial s$ is appreciable only where $\sin\phi \cos\phi$ is not small, but from figure 1 or (2.3), one sees that this occurs at small values of x (i.e. small s). Since the coefficient $(\partial \ln \bar{s}/\partial s)^{-1}$ in (3.6) is of the order of s, we conclude that the entire right side of (3·6) is small over the entire mixing layer. Neglect of this term on this basis is peculiar to high-altitude plumes, and does not occur when the inner and outer flows have equal stagnation pressures, as in the studies of Casaccio and Greenberg. Neglect of the right side of (3.6) does not make a description of the transverse pressure variation by (3.7) unnecessary, since it is required for a description of the state of the gas.

If the mixing layer is characterized by a binary mixture of non-reacting perfect gases with Lewis and Prandtl numbers of unity, the equations of species conservation and energy conservation assume forms similar to the momentum equation (Dorrance 1962). The resulting set of differential equations is

$$(Cf'')' + ff'' = 0, \quad (Cz')' + fz' = 0, \quad (Cg')' + fg' = 0, \qquad (3.8a,b,c)$$

where z is the mass fraction of jet species, g is $\bar{H}/\bar{H}_i$ and $\bar{H}$ is the stagnation enthalpy. The boundary conditions at the inner and outer edges of the mixing layer are, respectively,

$$f_i' = g_i = z_i = 1, \qquad (3.9a)$$

$$f_s' = \bar{u}_s/\bar{u}_i, \quad g_s = \bar{H}_s/\bar{H}_i, \quad z_s = 0, \qquad (3.9b)$$

and to the present order of accuracy, we may assume that

$$f = 0 \quad \text{at} \quad \eta = 0. \qquad (3.9c)$$

The energy and species equations have integral solutions of the Crocco type:

$$g = f'(1-g_s)/(1-f_s') + (g_s - f_s')/(1-f_s'), \qquad (3.10a)$$

$$z = (f' - f_s')/(1-f_s'). \qquad (3.10b)$$

With the approximation C = constant = 1, the mixing-layer equation (3.8) may be solved after the specification of the constant g_s and the variable $f_s'(s)$, obtained from analysis of the inviscid flow in the inner and outer shock layers, as shown below. Since the shock velocity in the inner shock layer is, to high accuracy, $\bar{q}_m \cos(\theta - \phi)$ and $\theta - \phi$ is everywhere small, a good approximation to the velocity across a thin inviscid inner shock layer is $\bar{q} = \bar{u} = \bar{u}_i = \bar{q}_m \cos(\theta - \phi)$. Unlike boundary-layer flow, velocity, species and enthalpy profiles are not necessarily coupled in shear layers. Conduction and diffusion may occur in the absence of

shear in the mixing layer. In this case, the Crocco integrals (3.10a, b) are not useful, since the denominators $1-f_s'$ vanish. Near this limit, it is appropriate to replace f by η in (3.8b, c), and also in (3.8a). All profiles then take on error-function forms by the analysis of § 7.

4. Mixing-layer boundary conditions, thermodynamic properties and controlling parameters

The velocity at the outer edge of the mixing layer is determined from the local pressure, stagnation enthalpy, shock relations and knowledge of where the local inviscid streamline crossed the outer shock. The shock crossing location is determined from mass conservation and the stream function (3.4).

$$\bar{\psi} = -\tfrac{1}{2}\bar{\rho}_\infty \bar{q}_\infty \tilde{\bar{r}}_0^2 = \left(2\int_0^{\bar{s}} \bar{\rho}_s \bar{\mu}_s \bar{u}_i \bar{r}_0^2 \, d\bar{s}\right)^{\frac{1}{2}} f(\eta_s); \tag{4.1a}$$

thus

$$\tilde{r}_0^2 = -f(\eta_s)\,[8M_\infty \tilde{s}(q_\infty^2 Re)^{-1}]^{\frac{1}{2}}. \tag{4.1b}$$

The integration of (3.8a) is begun with an estimate of $f_s' \simeq \bar{q}\cos\phi/\bar{q}_m\cos(\theta-\phi)$; then with $f(0) = 0$ and $f(\eta_i) = 1$, (3.8a) is integrated, and η_s is determined by a specified closeness of approach of f' to f_s' and f'' to 0. The associated $f(\eta_s)$ is used with (4.1b) to determine the shock crossing point for this streamline. Shock relations are applied at $\tilde{r}_0$ to determine the post-shock pressure and density:

$$\tilde{\rho}_{2s} = (\gamma_\infty+1)(\gamma_\infty-1)^{-1}[1+2(\gamma_\infty-1)^{-1}(M_\infty^2\sin^2\tilde{\phi})^{-1}]^{-1}, \tag{4.2a}$$

$$\tilde{p}_{2s} = 4(\gamma_\infty+1)^{-1}\sin^2\tilde{\phi}. \tag{4.2b}$$

The local density ρ_s is determined from (4.2), isentropic flow along the inviscid streamline, and the known local pressure p_s from (3.7). From the known stagnation enthalpy, local density and local pressure, one calculates u_s and hence f_s'. With this new f_s', (3.8a) is solved again, and the procedure is repeated until acceptable convergence is attained. A solution of (3.8a) immediately yields solutions to (3.8b, c), as shown in (3.10a, b).

The complete state of the gas is determined from solutions for p, f', g and z with the perfect-gas relation. Thus, in dimensionless form,

$$\bar{c}_p \bar{T}/\bar{H}_i = g - f'^2\cos^2(\theta-\phi) \tag{4.3a}$$

and

$$p/\rho = q_\infty^{-2}[g - f'^2\cos^2(\theta-\phi)]\,\bar{R}/\bar{c}_p, \tag{4.3b}$$

where

$$\bar{c}_p = z\bar{c}_{pj} + (1-z)\bar{c}_{p\infty}, \quad \bar{R} = zR_j + (1-z)\bar{R}_\infty.$$

The temperature and density in the mixing layer are calculated from the difference between the stagnation enthalpy and $\frac{1}{2}u^2$. This procedure becomes inappropriate near the inner edge of the layer, where this difference is very small. In this region, errors in temperature and density may be of the order of unity. However, temperatures here are, at most, a few hundredths of the stream stagnation and rocket chamber temperatures; consequently, this region is of little interest in studies of plume radiation. A proper calculation of the state of the gas at the inner edge of the mixing layer may be carried out which is similar to the

calculation at the outer edge, as described above. Mass conservation between streamlines yields

$$\bar{\psi} = \int_{\tilde{\theta}}^{\pi} \bar{\rho}_j \bar{q}_m \bar{r}^2 \sin\theta \, d\theta = \left(2\int_0^{\bar{s}} \bar{\rho}_s \bar{\mu}_s \bar{u}_i \bar{r}_0^2 \, d\bar{s}\right)^{\frac{1}{2}} f(\eta_i); \tag{4.4}$$

but from (1.1) and (1.2), (4.4) yields

$$\operatorname{erfc}(\Lambda\tilde{\beta}) = \left(1+\frac{1}{\gamma_j M_e^2}\right)\left(\frac{\bar{\rho}_e}{\bar{\rho}_c}\right)\frac{\Lambda}{B}\left(\frac{\bar{A}_e}{\bar{A}^*}\right) q_\infty^{-2}\left(\frac{2M_\infty \bar{s}}{Re}\right)^{\frac{1}{2}} f(\eta_i). \tag{4.5}$$

The place $\tilde{\theta}$ where the streamline at the inner edge η_i of the mixing layer crosses the inner shock is determined from (4.5). The post-shock pressure and density are computed from shock relations which are similar to (4.2a, b) and contain the pre-shock density and Mach number and the shock entry angle $\tilde{\theta}-\tilde{\phi}$. The pre-shock density is obtained from (1.2) and (1.3) in the following dimensionless form:

$$\tilde{\rho} = \frac{2Bq_\infty^2}{\pi \bar{r}^2} = \left(\frac{\bar{\rho}_c}{\bar{\rho}_e}\right)\left(\frac{\bar{A}^*}{\bar{A}_e}\right)\left(\frac{\bar{q}_m}{\bar{q}_e}\right)^2\left(1+\frac{1}{\gamma_j M_e^2}\right)\exp(-\Lambda^2\tilde{\beta}^2). \tag{4.6}$$

A^* and A_e are the nozzle throat and exit areas, respectively. The jet Mach number is related to the density by isentropic flow relations as

$$\tilde{M}^2 = M_e^2 (\bar{q}_m/\bar{q}_e)^2 (\tilde{\rho}/\tilde{\rho}_e)^{-(\gamma_j-1)}, \tag{4.7}$$

and this is the only appearance of the exit density. From the post-shock pressure and density, the computed pressure at the inner edge of the mixing layer and the isentropic flow along inviscid streamlines, the density and temperature at the mixing-layer edge are calculated. From these and the known stagnation enthalpy, the velocity at the inner edge is calculated. This completes the proper calculation of the state of the gas at the inner edge of the mixing layer. Since u_i is determined, it is a simple matter to use it to re-evaluate f_s' and repeat the above iterative solution for the mixing layer; this is done in the present work. Since u_i is very close to $\bar{q}_m\cos(\theta-\phi)$, no iteration on the value of u_i is required.

The solution in the plane of symmetry for the mixing layer of a high-altitude plume at a small angle of attack is seen above to depend on the following dimensionless parameters:

$$\alpha, \quad \bar{R}_j/\bar{R}_\infty, \quad \gamma_\infty, \quad \gamma_j, \quad M_e, \quad M_\infty,$$
$$q_\infty = \bar{q}_\infty/\bar{q}_m, \quad g_s = \bar{H}_\infty/\bar{H}_i, \quad Re = \bar{\rho}_\infty \bar{q}_m \bar{L}/\bar{\mu}_\infty,$$
$$\rho_e = \bar{\rho}_e/\bar{\rho}_\infty \quad \text{(for (4.7) only)}.$$

Inversion from $\bar{s}$, η co-ordinates to s, y co-ordinates is achieved using the relations (3.5). In hypersonic flight, the M_∞ dependence is weak, and the solution for the mixing layer depends primarily on the nozzle geometry, the stream- and jet-gas compositions, the angle of attack, $\bar{q}_\infty/\bar{q}_m$ and Re.

5. Inviscid layer analysis

Equations (4.1) and (4.5) may be used with streamline and shock-layer relations to generate the complete inviscid portions of the outer and inner shock layers, respectively. The outer-layer analysis proceeds from the outer edge of the mixing layer by differentiation of (4.1) with respect to η:

$$d\bar{r}_0^2 = -[8M_\infty \bar{s}(q_\infty^2 Re)^{-1}]^{\frac{1}{2}} f'(\eta)\, d\eta. \tag{5.1}$$

Since $f'(\eta_s)$ has been determined as discussed above, this provides the finite-difference form for a change in $\tilde{r}_0$, for a specified change in η. At the new $\eta = \eta_s + \Delta\eta$, the velocity u and hence $f'(\eta + \Delta\eta)$ are determined by the method discussed above, the local pressure $p(\eta + \Delta\eta)$ being determined from (3.7). Repeated use of this procedure generates the shock-layer solution to $\tilde{r}_0 = r_0$, which defines the local shock location. At the shock, the local pressure computed from (3.7) will be larger than that computed from shock relations with a shock inclination angle ϕ. This results because centrifugal pressure relief was neglected in the outer shock layer in the computation of $\bar{p}_{cs}$. A reasonable estimate of the local outer-shock slope may be obtained by selecting that slope which yields a post-shock pressure in agreement with (3.7). A completely analogous procedure applies to the inviscid portion of the inner shock layer, when (4.5) is used instead of (4.1). These solutions have not been carried out since they do not relate to the mixing layer. Mixing-layer boundary conditions are determined by solving inviscid layer equations along only one outer and one inner shock-layer streamline, as discussed above.

Local shock values of $f(\eta)$ are determined directly from (4.1) and (4.5) by replacing $\tilde{r}_0$ by r_0 and $\tilde{\theta}$ by θ. These stream-function values are useful as indications of the relative thickness of the inviscid shock layers and the mixing layer. From the outer-flow stream function (4.1a) the ratio of the mass of stream gas entrained in the mixing layer to that entrained within the outer shock is simply

$$\dot{M}_s/\dot{M}_{2s} = f(\eta_s)/f(\eta_{2s}). \tag{5.2a}$$

Similarly, from (4.4) the ratio of the mass of jet gas entrained in the mixing layer to that entrained within the inner shock is

$$\dot{M}_i/\dot{M}_{2i} = f(\eta_i)/f(\eta_{2i}). \tag{5.2b}$$

Solutions across the inviscid portions of the shock layers would complete the information necessary to test overall momentum conservation in the present analysis. Since momentum conservation is used in the inviscid analysis to generate (2.3), one may expect momentum to be very nearly conserved after the inclusion of a viscous mixing layer. It can be shown that overall mass and energy conservation is achieved exactly in the present formulation.

6. Further simplification

In addition to frequent use of the assumption of thin shock layers, the following assumptions have been used above to eliminate higher-order terms:

$$M_\infty^2 \gg 1, \quad M_\infty^2 \sin^2\phi \gg \gamma_\infty - 1, \quad M_\infty^2 \sin^2(\theta - \phi) \gg \gamma_j - 1. \tag{6.1}$$

Further simplification would result if $\cos(\theta - \phi)$ were replaced by unity. This would reduce the integral in (2.3) to a complementary error function, and simplify (4.3a,b) and the evaluation of u_i. Although this was not done, it would have introduced errors in state properties of less than 5%.

7. Solution along the dividing stream surface

With the allowed neglect of the pressure-gradient term in the momentum equation, the Crocco-type integral relations (3.10a,b) apply. Numerical solutions to (3.8a,b,c) for the broadest range of plausible boundary conditions for high-altitude plumes show that the surface $z = \frac{1}{2}$ lies very close to the dividing stream surface $\eta = 0$. Since here temperatures are relatively high because of conduction and viscous dissipation, and since here, also, the product $z(1-z)$ is a maximum, one may expect that the dividing stream surface is representative of the maximum reactivity for binary processes involving jet and stream gas species. Since this is a stream surface, non-equilibrium processes may be analysed most easily here. The state of the gas is determined simply with the assumption $z = \frac{1}{2}$ at $\eta = 0$, from (3.10) and (3.7).

$$f'_0 = \tfrac{1}{2}(1+f'_s), \quad g_0 = \tfrac{1}{2}(1+g_s), \quad p_0 = p_{cs}, \tag{7.1}$$

where the subscript zero indicates the dividing stream surface. The solution for the state at $\eta = 0$ is completed by (4.3a,b).

The outer-edge boundary condition f'_s may be determined approximately without solving the mixing-layer equations. An error-function approximation to f' results formally from the replacement of (3.8a) by

$$f''' + \eta f'' = 0. \tag{7.2}$$

The solution is

$$f' - f'_0 = \pm f''_0 (\tfrac{1}{2}\pi)^{\frac{1}{2}} \operatorname{erf}(\eta/\sqrt{2}), \tag{7.3}$$

where $\pm$ apply to $\pm\eta$, respectively. Edge boundary conditions ($\eta \to \pm\infty$) yield

$$f'_0 = \tfrac{1}{2}(1+f'_s), \quad f''_0 = (1-f'_s)(2\pi)^{-\frac{1}{2}} \tag{7.4a,b}$$

and integration of (7.3) yields

$$f_s = f'_s \eta_s + (1-f'_s)(2\pi)^{-\frac{1}{2}}. \tag{7.4c}$$

If the mixing layer is terminated at a small value ϵ of the ratio

$$(f'-f'_s)/(f'_0-f'_s) = \epsilon = [2(\pi\eta_s^2)^{-1}]^{\frac{1}{2}} e^{-\frac{1}{2}\eta_s^2}, \tag{7.5}$$

this defines the outer edge η_s of the mixing layer. The associated f_s, from (7.4c), is used with (4.1) to determine f'_s, as discussed above, with p_s replaced by p_{cs} with good accuracy.

It is noted that (7.4a) agrees with the assumption that $z = \frac{1}{2}$ at $\eta = 0$, which yielded (7.1). The above analysis thus provides an approximate, but consistent and complete description of the thermodynamic state on the dividing streamline, without solution of the mixing-layer equations.

8. Flow in the blunt nose region

Flow in the forwardmost portion of the mixing layer at high altitudes is complicated by a variety of phenomena, including some of the following: (a) nozzle boundary layers, (b) clustered nozzles, (c) vehicle shocks, (d) separated flow

caused by the 'corner' between the vehicle and the plume, and (*e*) rarefaction on the scale of the vehicle length. Inclusion of all the relevant phenomena would be extremely difficult, and inclusion of only some may not be meaningful. Their effects on the mixing layer may be important up to distances away from the nozzle of the order of the vehicle length. Over the altitude range between second-stage ignition and engine cut-off, the ratio of vehicle length to plume scale varies typically from 10^{-1} to 10^{-3}. At a normalized distance from the nozzle of 10^{-3}, the contact-surface inclination angle ϕ, from (2.3), is typically less than 70°; therefore, a detailed description of the plume mixing layer in the stagnation region ($\phi \sim 90°$) is unwarranted because of the above-mentioned disturbing influences.

9. Mixing-layer stability

In the forward region of the plume, where the contact-surface curvature is largest, the inviscid flow in the inner shock layer has a higher density and velocity than the adjacent flow in the outer shock layer. Since the inner flow is on the convex side of the contact surface, this surface is unstable. The mixing layer introduces a stabilizing influence, and the ratio of the mixing-layer thickness to the shock-layer thickness increases with increasing contact-surface curvature (i.e. decreasing r). The stability of the flow across this mixing layer has not been examined, and may have an important bearing on the applicability of all existing mixing-layer analyses.

10. Results

Errors introduced by the neglect of longitudinal pressure variations are greatest at intermediate values of θ, since the pressure gradient vanishes in the limits $\theta \to \frac{1}{2}\pi$ and $\theta \to 0$. The magnitude of these errors is shown by comparing a solution in which the pressure-gradient term, assumed constant (local similarity), was retained in (3.6) with a solution with the right side of (3.6) set to zero. This comparison is shown in figure 3 for engine and flight conditions representative of a large booster at an altitude above 100 km. The largest differences occur in the mixing layer near $\theta = 30°$; and the largest difference at $\theta = 30°$, shown in figure 3, corresponds to an error in temperature of the order of 10 % of the nozzle chamber temperature. Figure 3 illustrates that the surface $z = \frac{1}{2}$ is close to the dividing stream surface $\eta = 0$, a conclusion which is based on numerical results for a wide variety of boundary conditions.

Engine and flight conditions for a large booster operating at an altitude of 100 km are given in table 1. For such a large booster, one may expect a relatively thin mixing layer over the major portion of the plume. This is shown from the mixing-layer solution presented in figures 4–7. The ratio of the mass of jet gas entrained in the mixing layer to that contained in the shock layer and the equivalent ratio for the stream gas are shown in figure 4, as a function of polar angle, where $\eta_s = \eta_i \equiv 3{\cdot}0$. These ratios are small everywhere except at large θ ($> 60°$). For $\theta > 70°$, the computed mixing-layer thicknesses exceed the shock-layer thicknesses, indicating the onset of failure of the describing approximations. The

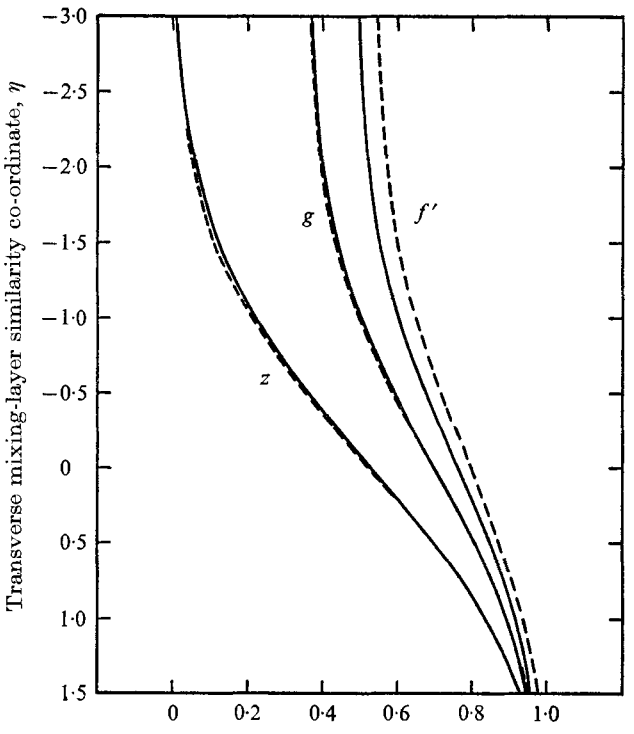

FIGURE 3. Order of error in mixing-layer properties from neglect of longitudinal pressure gradient (solid line), relative to properties calculated including this term (broken line). $f'_s = 0{\cdot}49$, $g_s = 0{\cdot}36$, $z_s = 0$.

Engine characteristics Input		Flight characteristics Input	
Vacuum thrust	$5{\cdot}15 \times 10^6$ N	Stream specific ratio	1·4
Jet specific-heat ratio	1·25	Stream temperature	210 °K
Exit Mach number	3·93	Stream molecular weight	29 amu
Exit temperature	1411 °K	Stream density	$4{\cdot}97 \times 10^{-7}$ kg/m^3
Jet molecular weight	13·1 amu	Vehicle speed	$3{\cdot}0 \times 10^3$ m/s
Exit density	$1{\cdot}86 \times 10^{-2}$ kg/m^3	Angle of attack	0
Computed		**Computed**	
Exit speed	$4{\cdot}16 \times 10^3$ m/s	Stream Mach number	10·3
Jet maximum speed	$5{\cdot}12 \times 10^3$ m/s	Stream stagnation enthalpy	$4{\cdot}71 \times 10^6$ m^2/s^2
Jet stagnation enthalpy	$1{\cdot}31 \times 10^7$ m^2/s^2	Stream stagnation temperature	4670 °K
D/T	0·171		
$L = 1{\cdot}52 \times 10^3$ m		Reynolds number $= 1{\cdot}72 \times 10^5$	

TABLE 1. High-altitude operating conditions for a large booster

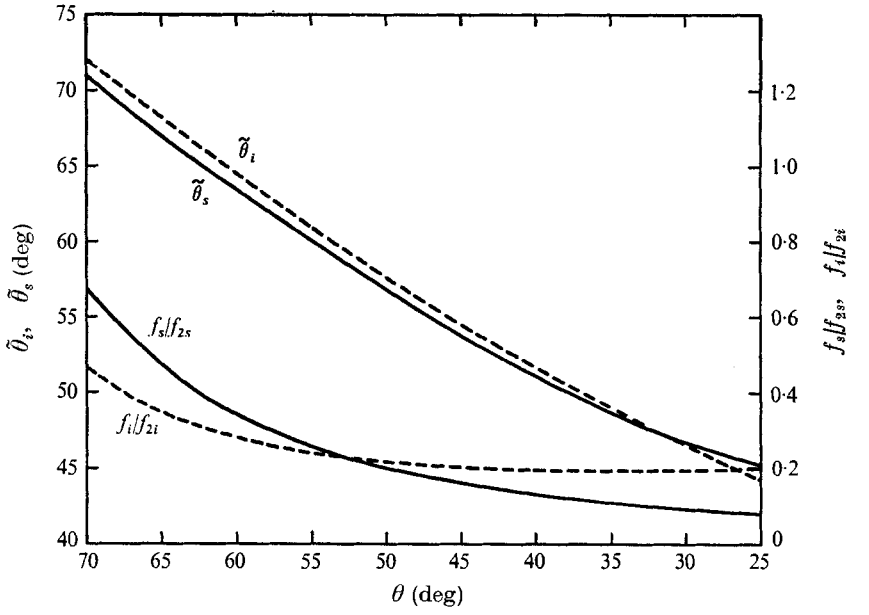

FIGURE 4. Shock energy angles for mixing-layer outer ($\tilde{\theta}_s$) and inner ($\tilde{\theta}_i$) edge streamlines, and outer (f_s/f_{2s}) and inner (f_i/f_{2i}) mass entrainment ratios, as a function of angle θ from the jet axis. See table 1 for the operating conditions. $Re = 1{\cdot}72 \times 10^5$.

Mixing-layer co-ordinates

θ	70	65	60	55	50
r	$3{\cdot}3 \times 10^{-3}$	$8{\cdot}3 \times 10^{-3}$	$1{\cdot}9 \times 10^{-2}$	$3{\cdot}8 \times 10^{-2}$	$7{\cdot}3 \times 10^{-2}$
θ	45	40	35	30	25
r	$3{\cdot}1 \times 10^{-1}$	$2{\cdot}2 \times 10^{-1}$	$3{\cdot}5 \times 10^{-1}$	$5{\cdot}4 \times 10^{-1}$	$8{\cdot}3 \times 10^{-1}$

table in figure 4, however, shows that the spatial extent of this fully viscous nose region is less than 6 m; furthermore, the solution does not apply in this negligibly small region for the additional reasons given in § 8. Also shown in figure 4, as a function of the mixing-layer station θ, are the shock entry points, in polar co-ordinates, for streamlines at the outer and inner edges of the mixing layer. The closeness of $\tilde{\theta}_s$ and $\tilde{\theta}_i$ to θ at large θ again implies relatively large mixing layers. It is interesting to note that the shock entry angles for streamlines at the mixing-layer edge at $\theta = 25°$ are about 45°. Thus, although the mixing layer is quite thin here (mass entrainment ratios of 0·195 and 0·067), inviscid stagnation streamline conditions would provide a very poor approximation to the outer-edge boundary conditions. The large Reynolds number in this example shows that the above statement applies in all cases where the mixing layer is laminar.

Velocity components $\bar{u}$ in the s direction are given in figure 5, *vs.* the polar angle θ. The notation for $\bar{u}$ from top to bottom is as follows: 'post-inner shock', 'inner mixing-layer edge', 'dividing streamline', 'post-outer shock', 'outer mixing-layer edge' and, finally, the value associated with the outer side of an inviscid contact surface, i.e. 'stagnation streamline'. The dividing-streamline velocity $\bar{u}_0$ is, from (7.1), the arithmetic mean of $\bar{u}_s$ and $\bar{u}_i$. The outer-edge

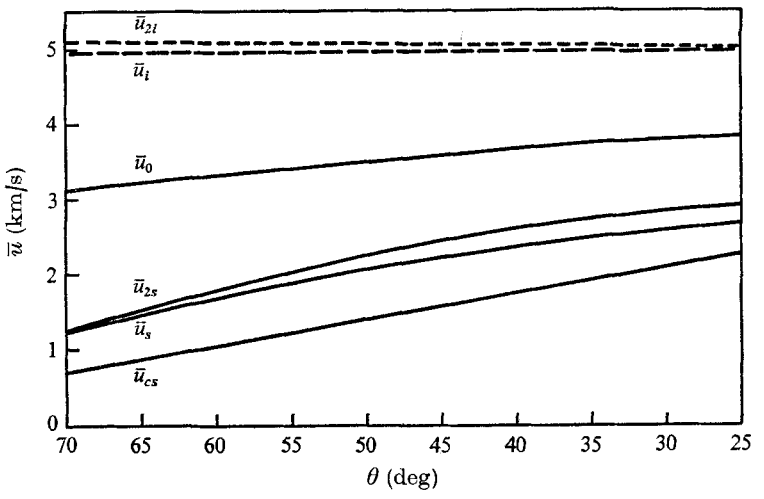

FIGURE 5. Velocity components $\bar{u}$ parallel to the mixing layer at five locations across the shock layers and mixing layer, and the velocity along the outer side of an inviscid contact surface, all as a function of angle θ from the jet axis. See table 1 for the operating conditions. $\bar{q}_m$ = 5·124 km/s, $\bar{q}_\infty$ = 3·0 km/s.

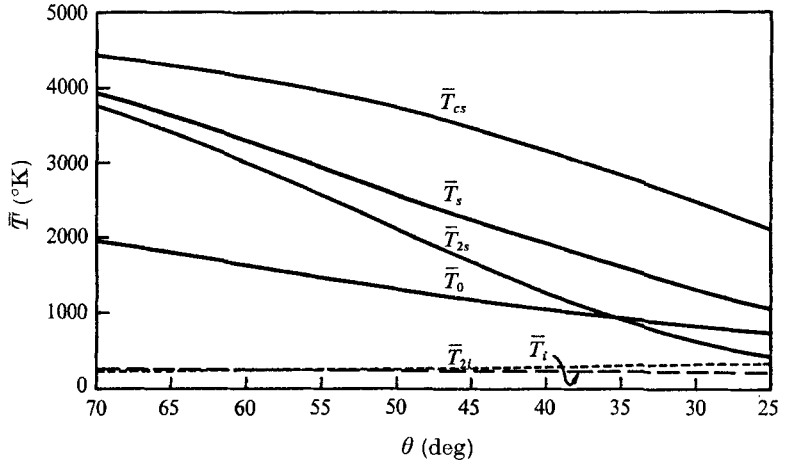

FIGURE 6. Temperature associated with the velocities in figure 5.
$\bar{T}_\infty$ = 210 °K, $\bar{T}_0$ = 4140 °K, $\bar{T}_e$ = 1411 °K.

velocity $\bar{u}_s$ is seen to differ significantly from the velocity $\bar{u}_{cs}$ on the inviscid stagnation streamline, thus illustrating further the inapplicability of $\bar{u}_{cs}$ as the outer-edge boundary condition, even at large Re. The closeness of the values of $\bar{q}_m$, $\bar{u}_{2l}$ and $\bar{u}_l$ support the statement that the velocities in inviscid portions of the jet are everywhere nearly constant and equal to $\bar{q}_m$.

Temperatures are presented as functions of the polar angle θ in figure 6, with the same subscript notation as in figure 5. Temperatures vary significantly across inviscid portions of the inner shock layer, but these variations are small compared with dividing-streamline temperatures $\bar{T}_0$. Significant differences between post-outer-shock temperatures and those at the mixing-layer edge

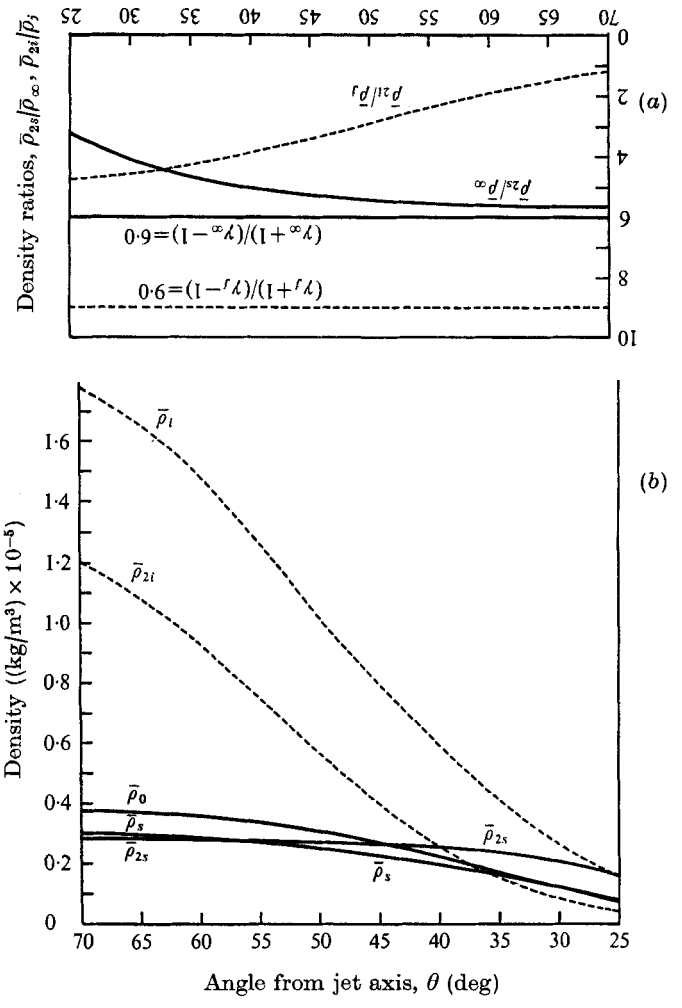

FIGURE 7. (*a*) Density ratios across outer and inner shocks and (*b*) densities associated with the velocities in figure 5. $\bar{\rho}_\infty = 4{\cdot}97 \times 10^{-7}$ kg/m^3, $\bar{\rho}_e = 1{\cdot}86 \times 10^{-2}$ kg/m^3.

are noted, and inviscid temperatures on the outer stagnation streamline bear little relationship to mixing-layer temperatures.

The densities presented in figure 7 have relatively high values in the inviscid portions of the inner shock layer and increase between the shock and the mixing-layer inner edge. Although jet densities, through dynamic pressures, are required in the construction of the mixing-layer location (2.3), the inner shock-layer densities contribute very weakly to the subsequent calculation of dividing-streamline properties, only through the calculation of the small variation between u_{2i} and u_i. Outer shock-layer densities are seen to be more representative of mixing-layer densities. Neither outer nor inner shock density ratios are as large as their strong-shock values of 6 and 9, respectively, shown in figure 7. For this reason, the Mach number dependencies were retained in the equations for the shock density ratio; however, it is again stressed that retention of jet Mach number

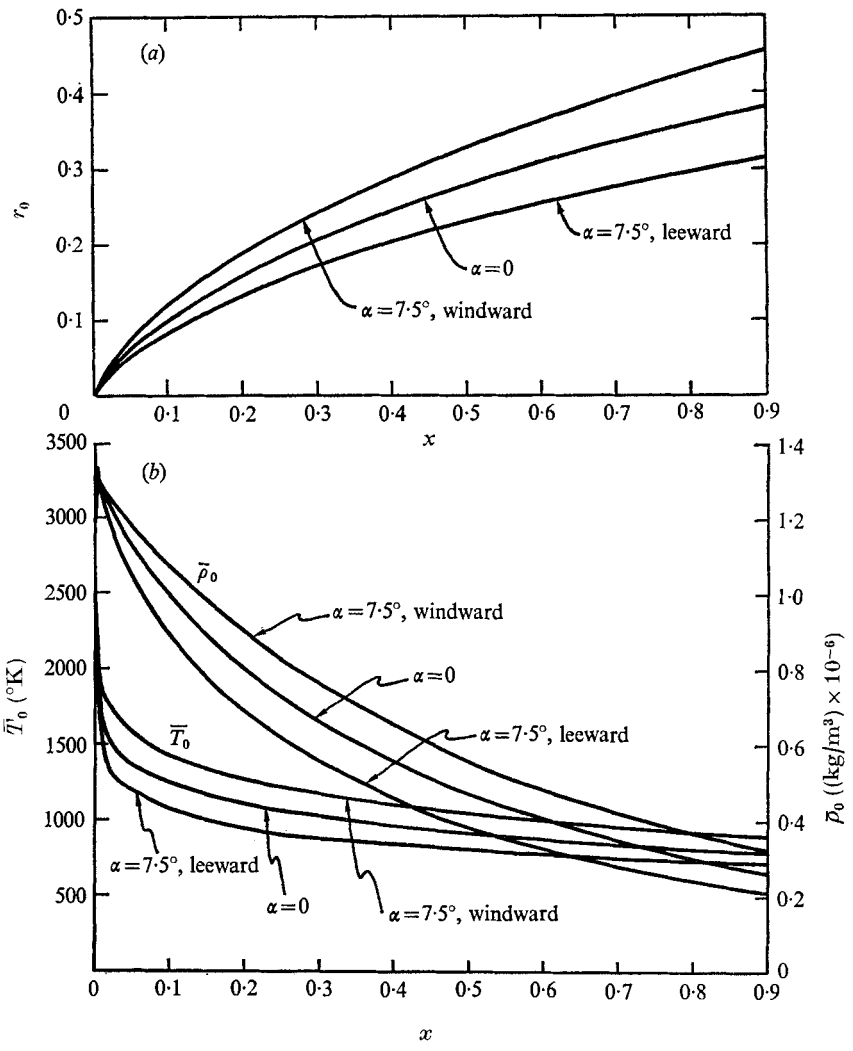

FIGURE 8. (*a*) Windward and leeward mixing-layer locations in the plane of symmetry, in a wind-axis co-ordinate system (x, r_0) for an angle of attack $\alpha = 7{\cdot}5°$, compared with the locations for $\alpha = 0$. Flight conditions are as in table 1, except for the following: $\bar{T}_\infty = 234$ °K, $\bar{\rho}_\infty = 2{\cdot}12 \times 10^{-7}$ kg/m³, $\bar{q}_\infty = 2{\cdot}6$ km/s, $\bar{T}_{t\infty} = 3600$ °K, $M_\infty = 8{\cdot}5$, $Re = 1{\cdot}23 \times 10^5$ and $\bar{L} = 2{\cdot}68$ km. The r_0 co-ordinate is the normalized cross-wind co-ordinate and the x co-ordinate is the normalized wind-axis co-ordinate. (*b*) Densities $\bar{\rho}_0$ and temperatures $\bar{T}_0$ along dividing streamlines associated with these mixing layers.

dependence and, hence, introduction of the nozzle-exit density, has a negligible effect on properties in the mixing layer.

The effects of the angle of attack α (between thrust axis and wind axis) on the mixing-layer location and properties are shown in figure 8. Engine and flight conditions in this example are as shown in table 1, except for the differences in flight conditions listed in figure 8. Windward and leeward mixing-layer (contact-surface) locations for $\alpha = 7{\cdot}5°$ are compared with the location for $\alpha = 0$. The associated temperatures and densities along the dividing streamlines are also

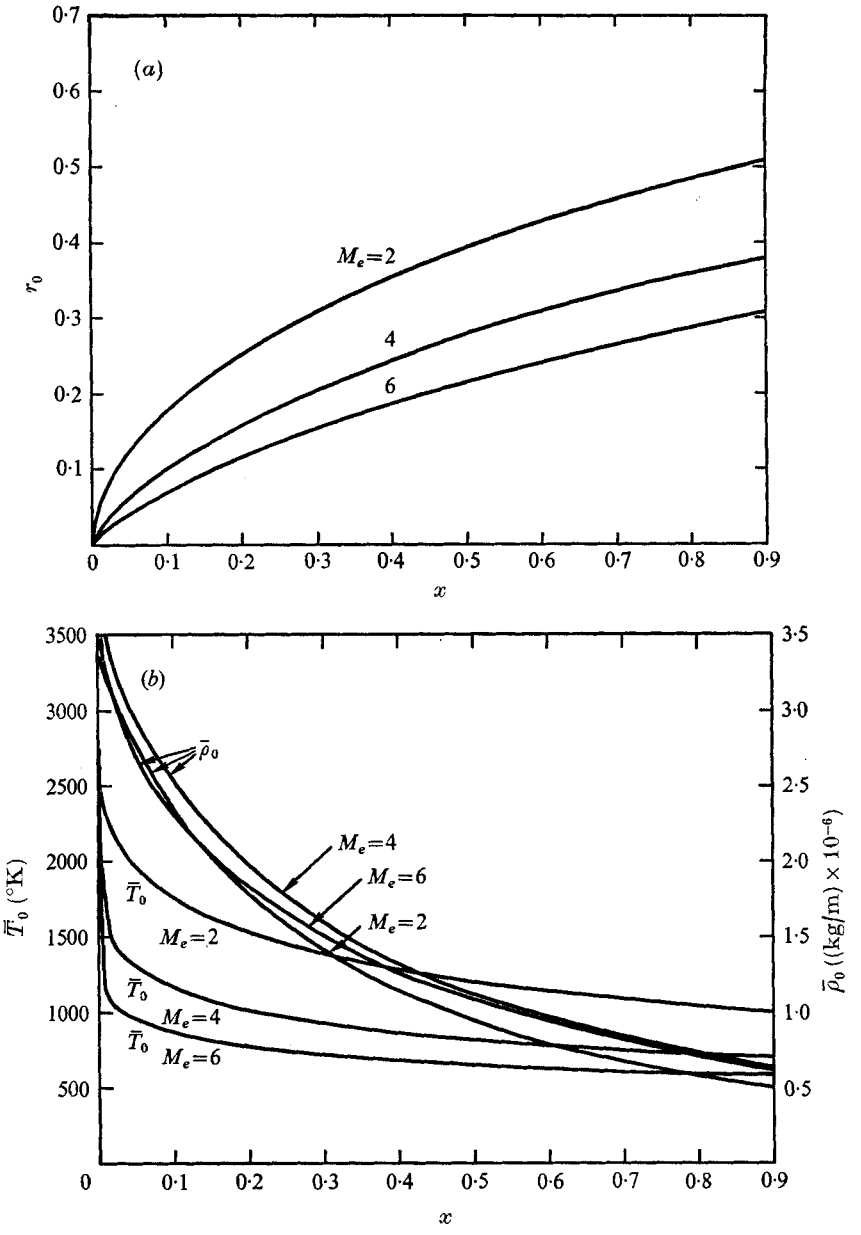

FIGURE 9. (*a*) Mixing-layer locations with thrust and chamber conditions constant for three values of nozzle-exit Mach number M_e. $Re = 1{\cdot}72 \times 10^5$, $\bar{L} = 1{\cdot}52$ km. See table 1 for flight characteristics and table 2 for engine characteristics. (*b*) Densities $\bar{\rho}_0$ and temperature $\bar{T}_0$ along dividing streamlines associated with these mixing layers.

shown in figure 8, *vs.* the normalized wind-axis co-ordinate. Differences of the order of 250 °K between windward and leeward mixing-layer temperatures are predicted for distances up to 1·0 km from the nozzle exit. This would cause strong differences in chemical and radiative processes, whose rates contain exponential temperature dependencies, even for this small and representative angle of attack.

			$M_e = 2$	$M_e = 4$	$M_e = 6$
Vacuum thrust	$5{\cdot}15 \times 10^6$ N	Exit temperature	2760	1380	754
Jet molecular weight	13·1 amu	Exit density (kg/m^3)	0·27	0·017	0·0015
Jet maximum speed	$5{\cdot}12 \times 10^3$ m/s	Exit speed (m/s)	$2{\cdot}96 \times 10^3$	$4{\cdot}19 \times 10^3$	$4{\cdot}64 \times 10^3$
Jet stagnation enthalpy	$1{\cdot}31 \times 10^7$ m^2/s^2	D/T	0·443	0·166	0·082

$\bar{L} = 1{\cdot}52 \times 10^3$ m Reynolds number $= 1{\cdot}72 \times 10^5$

TABLE 2. Engine characteristics for varying nozzle efficiencies

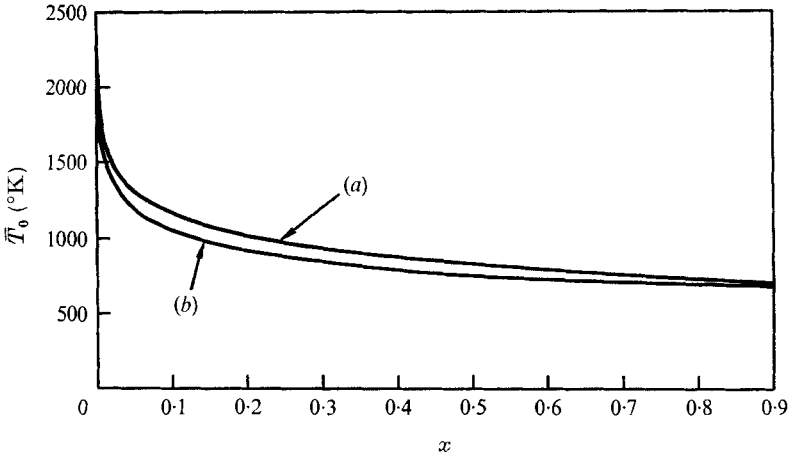

FIGURE 10. Dividing-streamline temperatures $\bar{T}_0$ as functions of normalized wind-axis co-ordinate x at two thrust levels. (*a*) $\bar{T} = 5{\cdot}15 \times 10^6$ N, $\bar{L} = 1{\cdot}52 \times 10^3$ m, $Re = 1{\cdot}72 \times 10^5$. (*b*) $\bar{T} = 5{\cdot}0 \times 10^4$ N, $\bar{L} = 1{\cdot}49 \times 10^2$ m, $Re = 1{\cdot}69 \times 10^4$. Other operating conditions are given in table 1.

Plume mixing-layer locations are shown in figure 9 for three values of the nozzle-exit Mach number for the flight conditions given in table 1 and the thrust and nozzle chamber conditions given in table 2. This comparison shows a relatively strong dependence of the plume transverse dimensions upon nozzle efficiency, with lower efficiencies associated with broader plumes. The associated dividing-streamline densities and temperatures in figure 9 show a rather weak density dependence and a strong temperature dependence on efficiency. Temperature differences of 600 °K are predicted for distances up to 1 km from nozzles with exit Mach numbers of 2·0 and 6·0, thus implying a strong dependence of chemical and radiative processes in the mixing layer on nozzle efficiency.

The sensitivity of mixing-layer properties to mixing-layer thickness was tested by comparing the solution for the conditions in table 1 with the solution with $\bar{T} = 5{\cdot}0 \times 10^4$N and all other conditions the same as in table 1. A reduction in thrust reduces $\bar{L}$ and hence Re, as shown in figure 10. The resulting relative thickening of the mixing layer changes the outer-edge boundary condition f'_s, as discussed in §4. Figure 10 shows that a thrust change of two orders of magnitude

causes small changes (less than 70° K) in dividing-streamline temperatures, and all other mixing-layer properties undergo correspondingly small changes.

Insensitivity of mixing-layer intensive properties to $\bar{T}$ implies insensitivity of normalized intensive properties to $\bar{L}$, and this allows a simple scaling of thrust and stream-density influences on overall properties. From figure 10 and the above discussion, one may expect this scaling to apply with good accuracy over two orders of magnitude in thrust and in stream density. If the thrust and stream density are varied, all other conditions being constant, the mixing-layer thickness [see equations (3.5)] and plume scale vary as

$$\bar{\delta} \propto \bar{\rho}_\infty^{-\frac{1}{2}} \bar{L}^{\frac{1}{2}}, \quad \bar{L} \propto \bar{T}^{\frac{1}{2}} \bar{\rho}_\infty^{-\frac{1}{2}}. \tag{10.1}$$

Consequently, the volume of the mixing layer varies as

$$\bar{V} \propto \bar{\delta} \bar{L}^2 \propto \bar{\rho}_\infty^{-\frac{1}{4}} \bar{T}^{-\frac{5}{4}}. \tag{10.2}$$

As an example of scaling of overall properties, the overall rate of progression of a two-body process would vary as

$$\bar{R} \propto \bar{\rho}_\infty^2 \bar{V} \propto \bar{\rho}_\infty^{\frac{1}{4}} \bar{T}^{-\frac{5}{4}}. \tag{10.3}$$

This provides an approximate altitude and thrust scaling relation which applies over a very broad range of operating conditions for boosters at high altitudes.

11. Summary

Highly underexpanded exhausts and hypersonic-vehicle Mach numbers associated with booster rockets at high altitudes allow major simplifications in the aerodynamic description of the mixing layer between the jet and ambient gases. The influence of the vehicle on the plume geometry is neglected; a far-field approximate description of the undisturbed jet core is employed; the thin mixing layer is centred along the inviscid contact surface, constructed by a Newtonian pressure balance between the inner and outer flows; consistent with the Newtonian approximation, shock layers are assumed sufficiently thin to allow equating of local shock slopes to the contact-surface slope. Mixing-layer equations in locally self-similar form for a binary mixture of ideal gases demonstrate that the neglect of the longitudinal pressure-gradient term introduces an error in temperature of the order of 10 % of the nozzle chamber temperature. With the assumption of Lewis and Prandtl numbers of unity, neglect of this pressure-gradient term allows Crocco integral solutions of the energy and species equations and relaxes certain restrictions on flow conditions for self-similarity pointed out by Greenberg.

The mixing-layer surface where the jet and stream mass concentrations are equal almost coincides with the dividing stream surface. Consequently, a simple and complete description of the state of the gas along the dividing streamline is provided in terms of mixing-layer boundary conditions. Boundary conditions are determined by (i) streamline tracing from the edges of the mixing layer to shock crossing points and (ii) use of shock relations and isentropic flow relations. The resulting description provides flow properties across the shock layers at seven

stations: pre- and post-inner shock, inner mixing-layer edge, dividing streamline, outer mixing-layer edge, and post- and pre-outer shock.

The following are the major results of the solutions presented. The speed in unmixed jet gas is everywhere very nearly equal to the jet maximum speed. Even when a small fraction of the shock-layer gas is entrained in the mixing layer, the inviscid velocity on the outer stagnation streamline provides a very poor approximation to the boundary condition at the outer edge of the mixing layer. Inner-shock density ratios are significantly lower than the limiting value of $(\gamma_j+1)/(\gamma_j-1)$, having, however, only a very weak influence on mixing-layer properties. Small angles between the thrust and wind axes cause pronounced differences between windward and leeward mixing-layer properties. The nozzle efficiency has a strong influence on mixing-layer temperatures, and the plume scale or plume Reynolds number has a rather weak influence on normalized mixing-layer intensive properties. This weak influence allows a simple and approximate scaling of mixing-layer overall properties. In the example given, the overall rate of progression of a two-body process depends on altitude and thrust as $\bar{R} \propto \rho_\infty^{\frac{1}{4}} \bar{T}^{\frac{5}{4}}$. It is evident from these studies that, apart from the inviscid construction of the mixing-layer location and the above volume scaling, mixing-layer properties are controlled primarily by stream- and jet-gas molecular properties and $\bar{q}_\infty$ and $\bar{q}_m$.

The author wishes to thank Dr Howard R. Baum, Dr Kevin S. Tait and Dr James S. Draper for many helpful discussions, and Dr Tait for computational support. The author gratefully acknowledges support by the Defense Advanced Research Projects Agency under contract DAAH0171 C 1291, monitored by the United States Army Missile Command.

REFERENCES

ALBINI, F. A. 1965 Approximate computation of underexpanded jet structure. *A.I.A.A. J.* **3**, 1535.

ALDEN, H. L. & HABERT, R. H. 1964 Gas dynamics of high-altitude rocket plumes. *MITHRAS Inc. Rep.* MC-63-80-R1.

ALDEN, H. L., HABERT, R. H. & HILL, J. A. F. 1963 Gas dynamics of high-altitude rocket plumes. *MITHRAS Inc. Rep.* MC-63-80.

ALTSHULER, S., MOE, M. M. & MOLUND, P. 1958 The electromagnetics of the rocket exhaust. *Space Tech. Lab. Inc. Rep.* GM-TR-0165-00397.

ASHKENAS, H. & SHERMAN, F. S. 1966 The structure and utilization of supersonic free jets in low density wind tunnels. In *Rarefied Gas Dynamics*, vol. 2 (ed. J. J. de Leeuw), pp. 84–105. Academic.

BOYNTON, F. P. 1967 Highly underexpanded jet structure: exact and approximate calculations. *A.I.A.A. J.* **5**, 1703.

BOYNTON, F. P. 1968 Exhaust plumes from nozzles with wall boundary layers. *J. Spacecraft*, **5**, 1143.

BOYNTON, F. P. 1971 Numerical calculations of viscous, high-altitude exhaust plume flow fields. *Res. Inst. Engng Sci. College of Engng, Wayne State University, Detroit, Michigan Rep.*

CASACCIO, A. 1963 Similar solutions for the turbulent compressible mixing of two streams with streamwise pressure gradient. *Republic Aviation Corp. Rep.* RAC 882A.

CHERNYI, G. G. 1961 *Introduction to Hypersonic Flow* (trans. & ed. R. F. Probstein), chap. 3. Academic.

DORRANCE, W. H. 1962 *Viscous Hypersonic Flow*, chap. 2. McGraw-Hill.

DRAPER, J. S. & MORAN, J. P. 1973*a* Evaluation of modelling and simulation of viscous effects in high-altitude plumes. *Proc. 7th JANNAF Plume Tech. Meeting.*

DRAPER, J. S. & MORAN, J. P. 1973*b* A study of wind tunnel simulation of high-altitude rocket plumes. *Air Force Rocket Propulsion Lab. Rep.* AFRPL TR-72-111.

GREENBERG, A. A. 1966 Laminar mixing of two streams in a pressure gradient. *M.I.T. Aerophys. Lab. Tech. Rep.* no. 117.

HARTMANN, J. & LAZARUS, F. 1941 The air-jet with a velocity exceeding that of sound. *Phil. Mag.* **31**, 35.

HAYES, W. D. 1947 On hypersonic similitude. *Quart. Appl. Math.* **5**, 105.

HAYES, W. D. & PROBSTEIN, R. F. 1959 *Hypersonic Flow Theory*, chap. 3. Academic.

HILL, J. A. F. & DRAPER, J. S. 1966 Analytical approximation for the flow from a nozzle into a vacuum. *J. Spacecraft*, **3**, 1552.

HILL, J. A. F. & HABERT, R. H. 1963 Gas dynamics of high-altitude missile trails. *MITHRAS Inc. Rep.* MC-61-18-R1.

HUBBARD, E. W. 1966 Approximate calculation of highly underexpanded jets. *A.I.A.A. J.* **4**, 1877.

JARVINEN, P. O. & DYNER, H. B. 1969 Rocket exhaust plume dimensions. *J. Spacecraft*, **6**, 1309.

JARVINEN, P. O. & HILL, J. A. F. 1970 Universal model for underexpanded rocket plumes in hypersonic flow. *Proc. 12th JANNAF Liquid Propulsion Meeting.*

LI, T. Y. & GEIGER, R. E. 1957 Stagnation point of a blunt body in hypersonic flow. *J. Aero. Sci.* **24**, 25.

LOCK, R. C. 1951 The velocity distribution in the laminar boundary layer between parallel streams. *Quart. J. Mech. Appl. Math.* **4**, 42.

MIRELS, H. & MULLEN, J. F. 1962 Expansion of gas clouds and hypersonic jets bounded by a vacuum. *Aerospace Corp. Rep.* TDR-169 (3230-12) TR-1.

MORAN, J. P. 1967 Similarity in high-altitude jets. *A.I.A.A. J.* **5**, 1343.

OWEN, P. L. & THORNHILL, C. K. 1948 The flow of an axially symmetric supersonic jet from a nearly sonic orifice into a vacuum. *Aero. Res. Counc. R. & M.* no. 2616.

ROSENBERG, N. W. HAMILTON, W. M., LOVELL, D. J. & BANG, B. A. 1961 High-altitude visible missile trails. In *Project Firefly* 1960, vol. 3. *Missile Trail Mechanisms, Air Force Camb. Res. Lab. Rep.* AFCRL 256 (III).

RUDMAN, S. 1973 Numerical study of highly underexpanded three dimensional plumes. *Adv. Tech. Lab. Rep.* ATL TR 184.

SEDOV, L. I. 1959 *Similarity and Dimensional Methods in Mechanics* (trans. & ed. M. Holt), chap. 4. Academic.

SIBULKIN, M. & GALLAHER, W. H. 1963 Far-field approximation for a nozzle exhausting into a vacuum. *A.I.A.A. J.* **1**, 1452.

SIMONS, G. A. 1972 Effect of nozzle boundary layers on rocket exhaust plumes. *A.I.A.A. J.* **10**, 1534.

TAYLOR, G. I. 1950 The formation of a blast wave by a very intense explosion *Proc. Roy. Soc.* A **201**, 159.

THOMSON, A. 1965 High-altitude rocket plume structure. *General Dyn. Corp. Convair Div. Rep.* GD-C-DBE65-023.

THOMSON, A. & HARSHBARGER, F. 1961 Some comments on the fluid dynamics of missile trails. In *Project Firefly* 1960, vol. 3. *Missile Trail Mechanisms, Air Force Camb. Res. Lab. Rep.* AFCRL 256 (III).

TING, L. 1959 On the mixing of two parallel streams. *J. Math. & Phys.* **38**, 153.

WILSON, K. H. 1973 Target phenomenology. Task I – Mixing layer analysis. *Lockheed Missiles & Space Co. Rep.* LMSC-B305172.